



## Performance analysis of forward osmosis processes from the integral equation theory

Albert S. Kim<sup>a,b,\*</sup>, Sung Woo Kim<sup>c</sup>

<sup>a</sup>Department of Civil and Environmental Engineering, University of Hawaii at Manoa, 2540 Dole Street, Honolulu, HI 96822, USA

<sup>b</sup>Department of Chemical Engineering, College of Engineering, Kyung Hee University, Gyeonggi-do 446-701, Korea

Email: albertsk@hawaii.edu

<sup>c</sup>Department of Physics and Astronomy, Dickinson College, Carlisle, PA 17013, USA

Received 15 June 2012; Accepted 24 September 2012

---

### ABSTRACT

We solved the Ornstein–Zernike integral equation to investigate non-linear behavior of osmotic pressure of solutions containing high concentrations of inorganic salts. Net interactions between molecules are assumed to be Lennard–Jones (LJ) potential, and various force fields were used to determine the potential parameters. Relationship between the LJ parameters and permeate flux are discussed, and relative significance of the osmotic pressure and diffusion coefficient on water flux in forward osmosis was investigated.

*Keywords:* Forward osmosis; Ornstein–Zernike equation; Virial coefficient; Osmotic pressure; Concentration dependent diffusivity

---

### 1. Introduction

Seawater desalination provides a promising way to achieve continuous water supply for agricultural, potable, or sanitary purposes, and reverse osmosis (RO) is an economically viable process to provide water for these purposes. On the other hand, forward osmosis (FO) has received recently close attention due to its low-energy consumption and availability of natural waters [1,2]. In addition to desalination, FO can be applied to concentrating sugar solutions [3] and dewatering of orange peel press liquor [4]. Important

issues in FO application include development of FO membranes of higher permeability [5–7], design of flat-sheet or hollow fiber modules, and high-performance draw solutes of high osmotic pressure and economic-regeneration/reconcentration [8–13]. For long-term operations, mitigation and prevention of FO membrane fouling must be another essential factor to minimize flux decline [14–21]. FO–RO hybrid systems were investigated for optimized operation of energy and cost savings [22–24]. Extensive reviews on FO research can be found elsewhere [25–28].

In contrast to the above-stated development of FO membrane materials and operational optimization, theoretical and modeling studies on FO phenomena are still in a burgeoning state after Lee et al. [29] and Loeb et al.

---

\*Corresponding author.

[30] studied pressure-retarded osmosis (PRO). Recent progress includes a modified theory that phenomenologically investigated impacts of concentration-dependent diffusivity and osmotic pressure on permeate flux [31], performance analysis [32–35], module design and membrane orientation [36,37], and concentration polarization due to physicochemical properties of saline solutions [38]. In addition, network modeling [39], computational fluid mechanics [40], and finite element method [41] were recently applied to model microscopic phenomena and process operation of FO.

In mass transport, osmotic pressure and diffusion coefficients are closely related, which are in general functions of solute concentration. Inter-molecular interactions significantly influence osmotic pressure by providing higher order virial coefficients. To the best of our knowledge, effects of inter-molecular interactions in PRO/FO processes on osmotic pressure and diffusion coefficients are not (fully) investigated. In this work, we used the random mixture theory as applied to the Ornstein–Zernike (OZ) equation, which is coupled with the hyper-netted chain (HNC) closure [42]. Effects of the non-linear osmotic pressure on water flux in FO and PRO processes are fundamentally studied using liquid-state statistical mechanics.

## 2. Background

After Loeb [43] studied energy production from concentrated brines using PRO, Lee et al. [29] developed the PRO theory as an alternative approach of solution-diffusion model: active membrane layer faces seawater and porous substrate faces fresh water. Loeb et al. [30] switched the membrane and substrate sides, facing to low and high concentrations, respectively, and called this configuration, “osmosis” mode. In contrast to Lee et al. [29]’s PRO mode, we in this study called Loeb et al. [30]’s osmosis mode FO mode. Schematic of concentration profiles of PRO and FO modes are shown in Fig. 1.

When concentration polarization occurs across the FO membrane as well as the porous substrate, it is often called internal concentration polarization (ICP) as opposed to the external concentration polarization (ECP) which often occurs in conventional pressure-driven membrane processes such as RO. In PRO of the concentrative ICP, the active layer faces the higher concentration solution; and in FO of the dilutive ICP, the active layer faces the lower concentration solution [44].

In the PRO mode of Fig. 1, the osmosis phenomena drives water to flow from low salt concentration (fresh water) to high salt concentration (seawater)

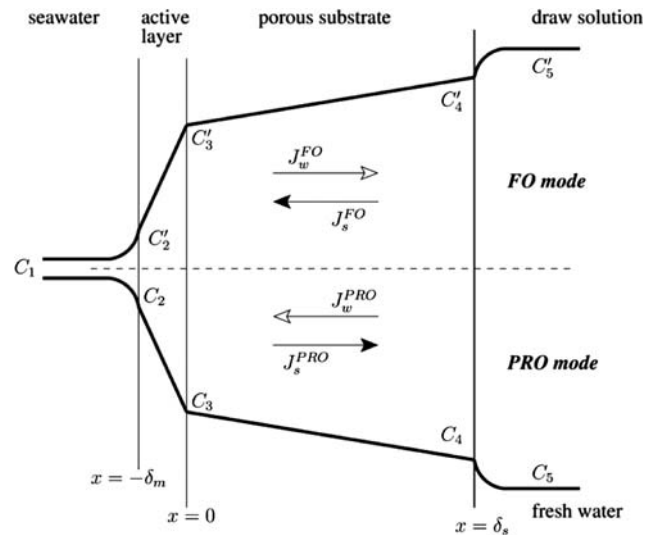


Fig. 1. A schematic representation of concentration polarization across a skinned membrane in FO for desalination (top part) and PRO for power generation (bottom part) using seawater of concentration  $C_1$ . In PRO mode,  $C_5$  is fresh water concentration, much lower than that of seawater, and  $C_2$ ,  $C_3$ , and  $C_4$  are concentrations at seawater-membrane, membrane-substrate, and substrate-fresh water interfaces. In FO mode,  $C'_5$  is concentration of draw solution, at least a few factor higher than  $C_1$ . Meanings of  $C'_2$ ,  $C'_3$ , and  $C'_4$  are similar to those in PRO mode. Directions of solvent and solute fluxes,  $J_w$  and  $J_s$ , are opposite to each other in both modes.

side, which results in interfacial concentrations of  $C_2 (< C_1)$  and  $C_4 (> C_5)$ , that is, ECP. In the porous substrate, the salt diffusion is hindered by the solid part of the substrate, which plays an impeding role of geometrical obstacles to diffusing molecules. Taking detoured routes, molecules spend more time in the porous media (than bulk spaces) so that effective diffusivity decreases. As a consequence, the concentration at the membrane-substrate interface,  $C_3$ , is noticeably higher than  $C_4$  of substrate-fresh water interface. The net concentration gradient across the top active layer is then proportional to  $C_2 - C_3$ , which is smaller than the overall concentration difference,  $C_1 - C_5$  (between bulk phases of seawater and fresh water). Through the membrane active layer, the water and solute fluxes were written as [29]

$$J_w = A\Pi_{\text{eff}} = A(\Pi_2 - \Pi_3) \quad (1)$$

and

$$J_s = B(C_2 - C_3) \quad (2)$$

where  $\Pi_{\text{eff}}$  is the effective osmotic pressure (i.e. net driving force of solvent flux),  $\Pi_i$  is osmotic pressure

of concentration  $C_i$  ( $i=1-5$ ), and  $A$  and  $B$  are permeabilities of water and solute, respectively. In a steady state, the solute mass flux in the porous region is

$$J_s = -D_s \frac{\epsilon}{\tau} \frac{\partial C}{\partial x} - J_w C \quad (3)$$

where  $D_s$  is the solute diffusivity, and  $\epsilon$  and  $\tau$  are porosity and (diffusive) tortuosity of the porous substrate [45]. Lee et al. [29] developed an analytic representation of a steady-state permeate flux:

$$J_w = K^{-1} \ln \frac{B + A\Pi_2 - J_w}{B + A\Pi_4} \quad (4)$$

where  $K$  was defined as “a measure of the resistance to salt transport in the porous substrate”:

$$K = \frac{\delta\tau}{D_s\epsilon} \quad (5)$$

Physically,  $K^{-1} = D_s\epsilon/\delta_s\tau$  has the same dimension of  $J_w$  and therefore can be regarded as a (conventional) mass transfer coefficient. During derivation of Eq. (4),  $C_3$  and  $\Pi_3$  were eliminated using the continuous boundary condition of the salt concentration at the membrane–substrate interface (at  $x=0$ ). Lee et al. [29] specifically assumed

$$\frac{\Pi_2 - \Pi_3}{\Pi_2 - \Pi_4} = \frac{C_2 - C_3}{C_2 - C_4} \quad (6)$$

which implies that the osmotic pressure is linearly proportional to concentration, that is, the van’t Hoff equation:  $\Pi = CRT$  where  $R$  is the universal gas constant and  $T$  is the absolute temperature. In recent papers that adopted Eq. (4) for theoretical improvement, it is often disregarded that Lee et al. [29]’s PRO theory is fundamentally limited by van’t Hoff’s equation for estimating osmotic pressure. Loeb et al. [30] indicated that Eq. (6) is “not-always-precise”. If so, accurate prediction of osmotic pressure in very high concentration is a crucial step to analyze PRO/FO performance in terms of  $J_w$ , as the osmotic pressure gradient is proportional to diffusion coefficient:  $D \propto \partial\Pi/\partial C$ .

Loeb et al. [30] investigated the efficiency of the osmosis-based power generation by positioning the low concentration solution on the active layer side of the membrane (i.e. switching from PRO mode to FO mode) and derived the water flux equation:

$$J_w = K^{-1} \ln \frac{B + A\Pi_2}{B + A\Pi_4 + J_w} \quad (7)$$

where  $\Pi_2 = \Pi(C_2)$  and  $\Pi_4 = \Pi(C_4)$  in Fig. 1. Mathematically,  $-J_w$  in the numerator of Eq. (4) is switched to  $+J_w$  in the denominator of Eq. (7), that is, from PRO to FO mode. As stated previously, Loeb et al. [30] recognized that the osmotic pressure varies in a non-linear manner with respect to salt concentration, but Eq. (7) presumes the validity of van’t Hoff’s equation in the FO mode processes.

Tan and Ng [31] investigated impacts of concentration polarization on flux behavior by taking into account the non-linear diffusion coefficient and osmotic pressure, which were represented as a power series and a quadratic function of solute concentration, respectively. OLI software (Steam Analyzer, OLI Systems, Inc. New Jersey, USA) was used to calculate  $D$  and  $\Pi$  as functions of  $C$ , and expansion coefficients were obtained by fitting simulation data from commercial software. Although Ng [31]’s modified theory begins with generalized Fick’s law of concentration-dependent diffusivity, the mass balance equation was not rigorously solved to derive an analytic solution for the permeate flux. Instead,  $k^* = \delta_s\tau/\epsilon$  was proposed as analogous to  $K$  of Lee et al. [29]’s original theory and arbitrarily expressed to include the non-linear impacts. Any fundamental relationship between  $\Pi$ ,  $D$ , and  $K^*$  was not obtained as they were quantified using fitting parameters of OLI simulation results.

### 3. Theory

Fundamental theories for FO/PRO phenomena can provide in-depth physical understanding of the solvent/solute transport and suggest essential operating parameters to optimize the processes in terms of water flux. To the best of our knowledge, the state-of-the-art theoretical developments are primarily based on Lee et al. [29]’s and Loeb et al. [30]’s work, which presumed the validity of van’t Hoff’s linear osmotic pressure generating constant diffusion coefficient. As stated previously, non-linear behaviors of osmotic pressure were investigated using commercial software (Steam Analyzer, OLI Systems, Inc. New Jersey, USA) [27,31]. Although the simulation results provide a method to analyze how water flux changes with solute species and concentrations, the effects of inter-molecular interactions on osmotic pressure have not been scrutinized. In this work, we combined the random mixture theory and OZ integral equation to calculate the radial distribution function (RDF) and the second virial coefficient of the osmotic pressure.

### 3.1. Osmotic pressure and diffusion coefficient

Generalized Fick's law for diffusive flux  $J_{\text{diff}}$  can be represented as

$$J_{\text{diff}} = -\frac{D_0}{RT} \frac{\partial \Pi}{\partial x} = -D(C) \frac{\partial C}{\partial x} \quad (8)$$

where  $D(C)$  is the generalized (concentration-dependent) diffusion coefficient

$$D(C) = D_0 \frac{\partial}{\partial C} \left( \frac{\Pi(C)}{RT} \right) \quad (9)$$

and  $D_0$  is that of dilute solution. In high concentrations, osmotic pressure is a non-linear function of  $C$ , expressed as a power series of concentration  $C$ :

$$\Pi = RT \sum_{k=1} b_k C^k = RT[C + b_2 C^2 + \dots] \quad (10)$$

where  $b_k$  is called  $k$ th virial coefficient. The first term  $RTC$  indicates van't Hoff's equation (i.e.  $b_1=1$ ), the second term with  $b_2$  originates from consecutive collisions between two solute molecules, which primarily influences the solute diffusion, and the third-term expresses effects of three-body collisions. In this work, the non-linear osmotic pressure is assumed to be a combination of entropy-increasing (CRT) and two-body collision ( $b_2 C^2 RT$ ) terms. This is because the three-body collisions between molecules are rare in aqueous systems. By definition of Eq. (9), the concentration-dependent diffusion coefficient is calculated as

$$D(C) = D_0(1 + 2b_2 C) \quad (11)$$

At low concentrations ( $b_2 C \ll 1$ ), the osmotic pressure and diffusion coefficient converge to the van't Hoff equation (CRT) and constant  $D_0$ , respectively. When multiple solute species are present in solution, the total molar concentration is

$$C = \sum_i C_i = C_1 + C_2 + \dots \quad (12)$$

and  $C_i = x_i C$  where  $x_i$  is a mole fraction of species  $i$ . In liquid-state statistical physics, the osmotic pressure is represented as

$$\frac{\Pi}{RT} = C - \frac{2\Pi}{3RT} \sum_{ij} C_i C_j \int_0^\infty g_{ij}(r) \frac{dU_{ij}(r)}{dr} r^3 dr \quad (13)$$

where  $U_{ij}$  and  $g_{ij}(r)$  are the potential energy and RDF of molecular species  $i$  and  $j$ , respectively. We assume

that inorganic species in high concentrations of PRO and/or FO processes are inert and have similar physicochemical properties. This leads to a simple approximation:  $g_{ij}(r) \simeq g(r)$ , which converts Eq. (13) to the original form of

$$\frac{\Pi}{RT} = C - \frac{2\Pi C^2}{3RT} \int_0^\infty g(r) \frac{dU(r)}{dr} r^3 dr \quad (14)$$

where  $U(r)$  is the mean potential of the mixture:

$$U(r) = \sum_{ij} x_i x_j U_{ij}(r) \quad (15)$$

The second virial coefficient is

$$b_2 = -\frac{2\pi}{3RT} \int_0^\infty g(r) \frac{dU(r)}{dr} r^3 dr \quad (16)$$

If solute mass fluxes of molecular species are on average similar, then the average mass flux is

$$J_i = -D_{0,i} \frac{\partial C_i}{\partial x} \approx J_s \quad (17)$$

and using Eq. (12)

$$J_s = -D_0 \frac{\partial C}{\partial x} \quad (18)$$

where

$$\frac{1}{D_0} = \sum_i \frac{1}{D_{0,i}} \quad (19)$$

In this random mixture theory, similar species are transformed into a single ideal species interacting with the mean potential  $U(r)$  and drifting with effective diffusivity  $D_0$  of Eq. (19).

### 3.2. Pair potentials

Specific form of the pair potential between molecule  $i$  and  $j$  consists of Coulombic (C) and Lennard-Jones (LJ) potentials:

$$U_{i,j}(r) = U_{ij}^C + U_{ij}^{LJ} \quad (20)$$

$$U_{ij}^C(r) = \frac{z_i z_j e^2}{r} \quad (21)$$

$$U_{ij}^{LJ} = 4\epsilon_{ij} \left[ \left( \frac{\sigma_{ij}}{r} \right)^{12} - \left( \frac{\sigma_{ij}}{r} \right)^6 \right] \quad (22)$$

where  $e$  is the elementary electric charge,  $z_i$  is the valence of species  $i$ , and  $\epsilon_{ij}$  and  $\sigma_{ij}$  are LJ parameters having dimensions of energy and distance, respectively. For interaction between two molecules of different species (i.e.  $i \neq j$ ), LJ parameters,  $\epsilon_{ij}$  and  $\sigma_{ij}$ , are calculated as geometric and arithmetic means, respectively, of those of species  $i$  and  $j$ :

$$\epsilon_{ij} = \sqrt{\epsilon_{ii}\epsilon_{jj}} \text{ and } \sigma_{ij} = \frac{1}{2}(\sigma_{ii} + \sigma_{jj}) \quad (23)$$

Ensuring the global charge neutrality, represented as  $\sum_k C_k z_k = 0$ , one can nullify the average influence of Coulombic potential:

$$\sum_{i,j} x_i x_j U_{ij}^C = 0 \quad (24)$$

and express the mean potential for the random mixture as a sum of molar-fraction-weighted LJ potentials

$$U(r) = \sum_{i,j} x_i x_j U_{ij}^{LJ}(r) = 4\bar{\epsilon} \left[ \left( \frac{\bar{\sigma}}{r} \right)^{12} - \left( \frac{\bar{\sigma}}{r} \right)^6 \right] \quad (25)$$

where

$$\bar{\epsilon} = \frac{[\sum_{i,j} x_i x_j \epsilon_{ij} \sigma_{ij}^6]^2}{\sum_{i,j} x_i x_j \epsilon_{ij} \sigma_{ij}^{12}} \quad (26)$$

and

$$\bar{\sigma} = \left[ \frac{\sum_{i,j} x_i x_j \epsilon_{ij} \sigma_{ij}^{12}}{\sum_{i,j} x_i x_j \epsilon_{ij} \sigma_{ij}^6} \right]^{\frac{1}{6}} \quad (27)$$

Negative differential of Eq. (25) with respect to  $r$  provides the mean force between two molecules:  $F(r) = -dU(r)/d(r)$ . The mean force is positive (repulsive) and negative (attractive) for  $r < r_{\min}$  and  $r > r_{\min}$ , respectively, where  $r_{\min} = \sqrt[6]{2}\bar{\sigma} = 1.122\bar{\sigma}$ . A larger  $\bar{\sigma}$  implies that effective length of intermolecular forces are longer, producing stronger interactions at given  $r$ . At  $r = r_{\min}$ , the mean potential is minimum and the mean force is zero. In summary, Eq. (25) implies that inorganic solute species of high concentration in PRO and FO processes are modeled as an ideal single component, which is electronically neutral and physicochemically characterized by the average LJ parameters of  $\bar{\epsilon}$  and  $\bar{\sigma}$ . These LJ parameters determine the virial coefficients and hence osmotic pressure.

### 3.3. Integral equation theory

With necessary LJ parameters known, the second virial coefficient  $b_2$  needs to be calculated using principles of statistical mechanics. Molecular dynamics and Monte Carlo simulations are standard techniques to investigate physical and chemical properties of specific materials in various phases including liquids. Integral equation theory for the random mixture, on the other hand, provides a convenient and fast method to calculate  $b_2$  and investigate properties of the high concentration solution.

If the fluid is uniform and isotropic, the OZ-relation is

$$h(\mathbf{r}) = c(\mathbf{r}) + \rho \int c(|\mathbf{r} - \mathbf{r}'|)h(\mathbf{r}')d\mathbf{r}' \quad (28)$$

which is a convolution integral of the direct correlation function  $c(r)$ , where  $h(r) = g(r) - 1$  is the total correlation function, and  $\rho$  is the number density of solute molecules. On taking the Fourier transformation of both sides of Eq. (28), one obtains

$$\hat{H}(\mathbf{k}) = \frac{\hat{C}(\mathbf{k})}{1 - \rho \hat{H}(\mathbf{k})\hat{C}(\mathbf{k})} \quad (29)$$

where

$$\hat{H}(\mathbf{k}) = \int h(\mathbf{r})\exp(-i\vec{k} \cdot \vec{r})d\mathbf{r} \quad (30)$$

and

$$\hat{C}(\mathbf{k}) = \int c(\mathbf{r})\exp(-i\vec{k} \cdot \vec{r})d\mathbf{r} \quad (31)$$

Eq. (29) requires a relationship between  $c(r)$  and  $h(r)$ , called a closure. We selected the HNC closure, expressed as

$$c(\mathbf{r}) = h(\mathbf{r}) - \beta U(\mathbf{r}) - \ln(h(\mathbf{r}) + 1) \quad (32)$$

where  $\beta = 1/k_B T$  and  $k_B$  is the Boltzmann constant. With the molecular interaction  $U(r)$ ,  $c(r)$  and  $h(r)$  can be interactively solved using Eqs. (29)–(32). For dilute systems, the correlations in the positions of the molecules are only due to the potential engendered by the reference particle. In this case, the Boltzmann distribution law gives an approximate expression:  $h(r) \approx \exp[-\beta U(r)] - 1$ , which is frequently used as an initial guessed function of  $h(r)$  of a higher concentration. Detailed algorithm to numerically solve the OZ

equation using a closure relationship can be found elsewhere [42].

## 4. Results and discussion

### 4.1. Radial distribution function

We selected NaCl to model saline solutions of various concentrations, which included the standard seawater concentration of 0.59 M (as NaCl) and draw solution concentrations of FO as high as 5.0 M. Specific pair potentials are for sodium–sodium ( $\text{Na}^+ - \text{Na}^+$  or 1:1), sodium–chlorine ( $\text{Na}^+ - \text{Cl}^-$  or 1:2), and chlorine–chlorine ( $\text{Cl}^- - \text{Cl}^-$  or 2:2), where ion numbers are, for simplicity, denoted as 1 for  $\text{Na}^+$  and 2 for  $\text{Cl}^-$ . Molar fractions are  $x_1 = x_2 = 0.5$  because NaCl completely dissolves in water with equal molarity of  $\text{Na}^+$  and  $\text{Cl}^-$ . Table 1 summarizes LJ parameters of NaCl from six force fields for molecular dynamics simulations: GROMACS [46], CHARMM [47], OPLS [48], X-PLOR [49], AMBER [50], and Smith-94 [51]. Coupled parameters of  $\epsilon_{12}$  and  $\sigma_{12}$  are calculated using Eqs. (26) and (27), that is,  $\epsilon_{12} (= \sqrt{\epsilon_{11}\epsilon_{22}})$  and  $\sigma_{12} (= \frac{1}{2}(\sigma_{11} + \sigma_{22}))$ .

The mean pair potential for NaCl solution without the Coulombic potential (dropped because of the global charge neutrality) is  $U(r) = 0.25[U_{11}^{\text{LJ}} + 2U_{12}^{\text{LJ}} + U_{22}^{\text{LJ}}]$  where  $U_{12}^{\text{LJ}} = U_{21}^{\text{LJ}}$ . Since the molar concentration of pure water is 55.0 M, the mole fraction of 5 M as NaCl draw solution is below 0.1. This implies that the RDF is not sensitive to the number concentration  $\rho$  ( $=N_A C$ ) in OZ equation (28), where  $N_A$  is Avogadro's number. We calculated RDFs with concentrations from 1.0 to 5.0 M and found that results are almost indistinguishable in terms of RDF shapes and (more importantly) values of  $b_2$ . Fig. 2 shows RDFs of the six force fields calculated for 5.0 M NaCl concentration. RDFs of X-PLOR, CHARMM, and Smith-94 show three highest peaks, which are the same order of their  $\bar{\epsilon}$  values: X-PLOR (77.05 cal/mol), CHARMM (59.58 cal/mol), and Smith-94 (57.24 cal/mol). The order of  $\bar{\sigma}$  values of CHARMM (3.916 Å), X-PLOR (4.075 Å), and Smith-94

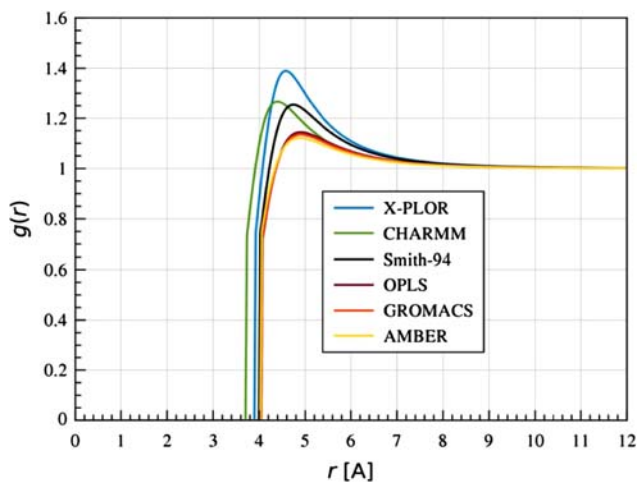


Fig. 2. RDFs with  $C_{\text{NaCl}} = 5.0$  M. On-set positions of  $g(r)$  are CHARMM (3.7358 Å), X-PLOR (3.9276 Å), Smith-94 (4.0263 Å), AMBER (4.0558 Å), OPLS (4.0744 Å), and GROMACS (4.0760 Å), which are all smaller than their  $\bar{\sigma}$  values listed in Table 1.

(4.222 Å) is reflected the sequence of their on-set positions, below which the probability that molecules are found at distance  $r$  from a reference molecule is zero and hence  $g(r)$  is. OPLS, GROMACS, and AMBER have similar values of  $36.2 > \bar{\epsilon} > 31.3$  cal/mol and  $4.4 > \bar{\sigma} > 4.3$  Å, and so they show similar  $g(r)$  curves in Fig. 2.

Table 2 summarizes the second virial coefficient  $b_2$  and  $b_2 RT$  calculated using Eq. (14) for NaCl solution of 5 M. As described earlier, we calculated  $b_2$  for  $C = 1, 2, 3, 4,$  and  $5$  M and found that all  $b_2$  values are within 1.0% difference from that of  $C = 5$  M (data not shown). X-PLOR provides the highest  $\bar{\epsilon}$  ( $=77.1$  cal/mol) as well as  $b_2$  ( $=0.03426$  lit/mol) and its  $\bar{\sigma}$  ( $=4.075$  Å) is the second to the least value 3.916 Å (CHARMM). A higher  $\bar{\epsilon}$  of the mean molecular interaction increases the second virial coefficient  $b_2$  and hence the osmotic pressure; and the effect of  $\bar{\sigma}$  seems to be smaller than that of  $\bar{\epsilon}$ . Smith-94 has lower  $\bar{\epsilon}$  ( $=57.2$  cal/mol) and higher  $\bar{\sigma}$  ( $=42.22$  Å) than those of CHARMM ( $\bar{\epsilon} = 59.6$  cal/mol

Table 1

LJ parameters for  $\text{Na}^+$  and  $\text{Cl}^-$  (denoted as 1 and 2, respectively) obtained from molecular dynamics force fields and mean values calculated using Eqs. (26) and (27). Units of  $\epsilon$ 's and  $\sigma$ 's are cal/mol and Å, respectively

	X-PLOR		CHARMM		Smith-94		OPLS		GROMACS		AMBER	
	$\epsilon_{ij}$	$\sigma_{ij}$										
11	100.0	2.730	46.9	2.430	100.1	2.350	2.8	3.330	14.8	2.575	2.8	3.328
22	150.0	4.276	150.0	4.045	129.9	4.400	117.8	4.417	106.4	4.448	100.0	4.401
12	122.5	3.503	83.9	3.237	114.0	3.375	18.2	3.874	39.6	3.384	16.6	3.865
mean	77.1	4.075	59.6	3.916	57.2	4.222	36.2	4.364	34.2	4.366	31.3	4.344

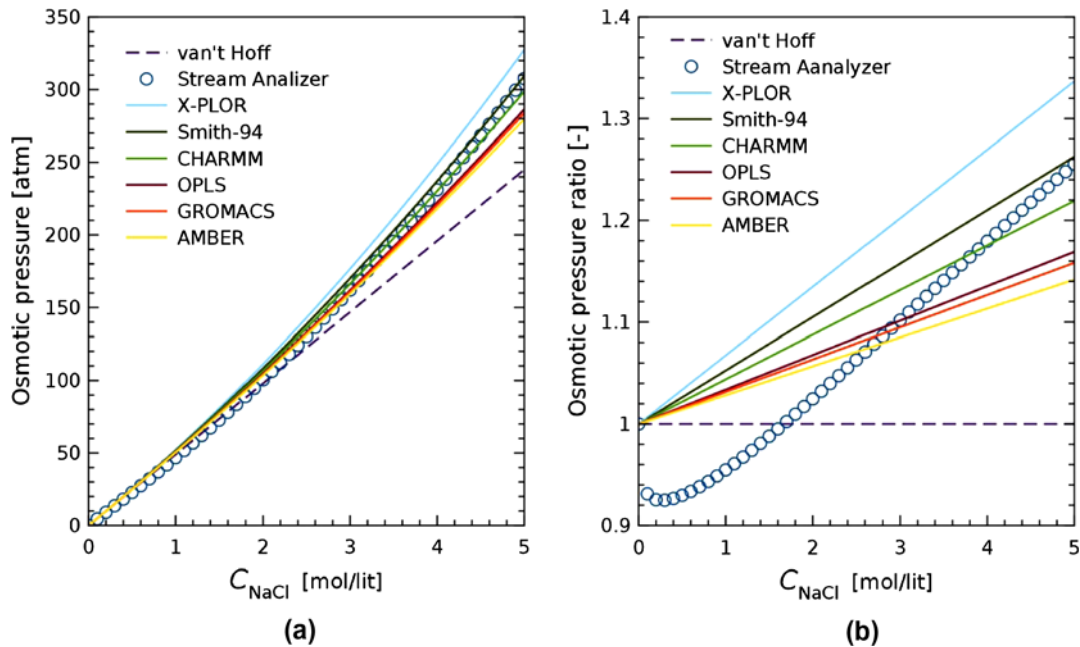


Fig. 3. Comparison of (a) osmotic pressure and (b) osmotic pressure ratio with respect to van't Hoff's equation as functions of NaCl concentration.

and  $\bar{\sigma}=3.916\text{\AA}$ ), and gives the second highest  $b_2$  ( $=0.02671$  lit/mol) followed by that of CHARMM ( $b_2=0.02230$  lit/mol).  $g(r)$  shapes of CHARMM and Smith-94 can be compared in terms of their peak positions and heights. Because  $\bar{\epsilon}$  values of Smith and CHARMM are similar, larger  $\bar{\sigma}$  ( $=4.222$  Å) of Smith-94 than that of CHARMM ( $\bar{\sigma}=3.916\text{\AA}$ ) seems to contribute to higher second virial coefficient than that of CHARMM. Comparing  $\bar{\epsilon}$ ,  $\bar{\sigma}$ , and  $b_2$  values of X-PLOR, Smith-94 and CHAMRR, one can conclude that  $b_2$  primarily increases with  $\bar{\epsilon}$ , followed by  $\bar{\sigma}$ . Conversely saying, when draw solutes for the FO processes are sought, ones with higher  $\bar{\epsilon}$  and then larger  $\bar{\sigma}$  will surely increase the osmotic pressure and its gradient (i.e.  $\Pi$  and  $\partial\Pi/\partial C$ ) and therefore enhance water flux.

#### 4.2. Osmotic pressure

Fig. 3 shows osmotic pressure curves predicted using the six force fields, OLI software, and van't Hoff's equation. In Fig. 3(a), calculation results show

higher osmotic pressures than one predicted using van't Hoff's equation. X-PLOR predicted higher osmotic pressure than that of OLI, which is similar to those of Smith and CHARMM. As expected, OPLS, GROMACS, and AMBER provide lower osmotic pressure than those of other force fields. Fig. 3(b) shows ratios of osmotic pressures to that of van't Hoff's equation. Slopes of straight lines in Fig. 3(b) represent  $b_2$  values of the force fields. Interestingly, osmotic pressure ratio predicted using Stream Analyser (SA) software from OLI is smaller than 1.0, in other words,  $\pi_{\text{OLI}}(C) \leq \text{RTC}$  for  $C \lesssim 1.6$ . For higher concentrations ( $3\text{M} < C < 5\text{M}$ ), SA, Smith-94, and CHARMM give similar values, specifically indicating that the osmotic pressure increases about 20% from van't Hoff's equation near  $C=4\text{M}$ .

#### 4.3. Diffusion coefficient and permeate flux: implications

In this section, we qualitatively discuss effects of  $\pi(C)$  and  $D(C)$  on water flux in FO. Comparing Eqs. (10) and (11), one can notice that the slopes of

Table 2  
The second virial coefficient  $b_2$  and  $b_2RT$  at  $T=298.5\text{K}$

	X-PLOR	Smith-94	CHARMM	OPLS	GROMACS	AMBER
$b_2$ [1/M]	0.03426	0.02671	0.02230	0.01719	0.01609	0.01440
$b_2RT$ [atm/M <sup>2</sup> ]	0.8250	0.6433	0.5370	0.4140	0.3875	0.3468

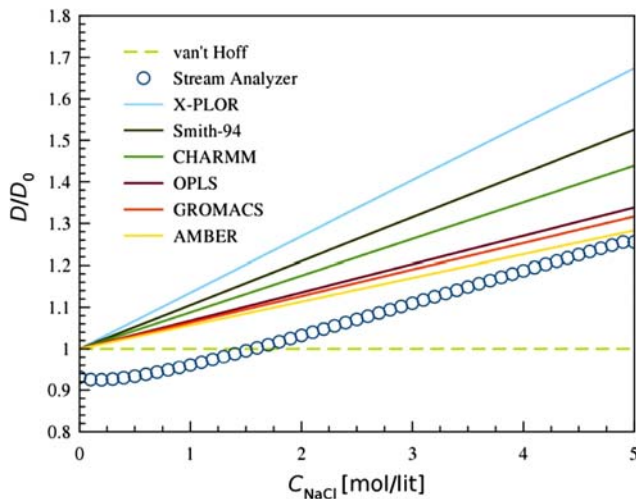


Fig. 4. Diffusion coefficient of NaCl random mixture vs. NaCl concentration.  $D_0$  of NaCl can be calculated as  $1.372 \times 10^{-9} \text{ m}^2/\text{s}$ , which is  $\left(\frac{1}{D_{\text{Na}^+}} + \frac{1}{D_{\text{Cl}^-}}\right)^{-1}$  where  $D_{\text{Na}^+} = 3.334 \times 10^{-4} \text{ m}^2/\text{s}$  and  $D_{\text{Cl}^-} = 2.032 \times 10^{-9} \text{ m}^2/\text{s}$ .

dimensionless diffusivity  $D(C)/D_0$  for the six force fields are twice those of osmotic pressure ratios (shown in Fig. 4). The dimensionless diffusivity of SA is smaller than those of any other force fields; and the slope of SA looks parallel to that of CHARMM, but smaller than 1.0 when  $C \lesssim 1.6$ . All the simulation results shown in Fig. 4 indicate that diffusivity noticeably increases with concentration if the salt concentration is greater than approximately 3.0 M.

Stronger molecular interaction produces higher  $b_2$  and hence higher  $\Pi$  (than that predicted by van't Hoff equation). Functional dependence of  $\Pi$  and  $D$  on concentration  $C$  are quadratic and linear, respectively. Although a higher  $C$  significantly increases  $\Pi$  as a driving force of the permeate flux in PRO and FO, its impacts must be gradual because  $J_w$  increases logarithmically with respect to  $\Pi$  in Eqs. (4) and (7):  $J_w \propto \ln \Pi_{\text{high}}$ . On the other hand,  $J_w$  is directly proportional to the diffusion coefficient:  $J_w \propto K^{-1} \propto D_0$ . Solutes with higher  $b_2$  can noticeably increase the permeate flux by enhancing primarily  $D(C)$  and secondarily  $\Pi(C)$ . Because  $K^{-1}$  is the crucial factor that determines an order of magnitude of water flux, solutes of higher  $D_0$  will produce higher water flux. Higher diffusivity will enhance back-diffusion away from the membrane interfaces, diminish ICP, and finally enhance water flux.

## 5. Conclusions

We applied OZ integral equation theory to calculate the second virial coefficient of the osmotic pressure of solutions containing inert inorganic species.

Six standard force fields were used to calculate  $b_2$  and compared with OLI software and van't Hoff's equation. The osmotic pressure was calculated as a quadratic function of the solute concentration. Influence of  $b_2$  to the permeate flux are through the osmotic pressure and diffusion coefficient: the former is less important as it logarithmically increases with respect to concentration, but the latter increases linearly. Simulation results imply that desired draw solutes should have higher  $\bar{\epsilon}$  and larger  $\bar{\sigma}$  with the global charge neutrality presumed.

## Acknowledgments

This research was supported by Kyung Hee University International Scholar Program and Undergraduate Intern Program of Dickson College. We appreciate Prof. Tzahi Cath at the Colorado School of Mines for providing simulation data of NaCl osmotic pressure using OLI software; and Prof. Yong Taek Lee and Ms. Min Jung Kim at Kyung Hee University for providing necessary information and running model simulations, respectively.

## References

- [1] V. Yangali-Quintanilla, Z. Li, R. Valladares, Q. Li, G. Amy, Indirect desalination of Red Sea water with forward osmosis and low pressure reverse osmosis for water reuse, *Desalination* 280(1–3) (2011) 160–166.
- [2] D. L. Shaffer, N.Y. Yip, J. Gilron, M. Elimelech, Seawater desalination for agriculture by integrated forward and reverse osmosis: Improved product water quality for potentially less energy, *J. Membr. Sci.* 415–416 (2012) 1–8.
- [3] E.M. Garcia-Castello, J.R. McCutcheon, M. Elimelech, Performance evaluation of sucrose concentration using forward osmosis, *J. Membr. Sci.* 338(1–2) (2009) 61–66.
- [4] E.M. Garcia-Castello, J.R. McCutcheon, Dewatering press liquor derived from orange production by forward osmosis, *J. Membr. Sci.* 372(1–2) (2011) 97–101.
- [5] Y.-X. Jia, H.-L. Li, M. Wang, L.-Y. Wu, Y.-D. Hu, Carbon nanotube: Possible candidate for forward osmosis, *Sep. Purif. Tech.* 75(1) (2010) 55–60.
- [6] N. Ma, J. Wei, R. Liao, C.Y. Tang, Zeolite-polyamide thin film nanocomposite membranes: Towards enhanced performance for forward osmosis, *J. Membr. Sci.* 405–406 (2012) 149–157.
- [7] J. Wei, X. Liu, C. Qiu, R. Wang, C.Y. Tang, Influence of monomer concentrations on the performance of polyamide-based thin film composite forward osmosis membranes, *J. Membr. Sci.* 381(1–2) (2011) 110–117.
- [8] J.R. McCutcheon, R. McGinnis, M. Elimelech, Desalination by ammonia-carbon dioxide forward osmosis: Influence of draw and feed solution concentrations on process performance, *J. Membr. Sci.* 278(1–2) (2006) 114–123.
- [9] R. McGinnis, J.R. McCutcheon, M. Elimelech, A novel ammonia-carbon dioxide osmotic heat engine for power generation, *J. Membr. Sci.* 305(1–2) (2007) 3–19.
- [10] A. Achilli, T.Y. Cath, A.E. Childress, Selection of inorganic based draw solutions for forward osmosis applications, *J. Membr. Sci.* 364(1–2) (2010) 233–241.
- [11] M. Sairam, E. Sereewatthanawut, K. Li, A. Bismarck, A.G. Livingston, Method for the preparation of cellulose acetate flat sheet composite membranes for forward osmosis—desalination using  $\text{MgSO}_4$  draw solution, *Desalination* 273(2–3) (2011) 299–307.

- [12] T.-W. Kim, Y. Kim, C. Yun, H. Jang, W. Kim, S. Park, Systematic approach for draw solute selection and optimal system design for forward osmosis desalination, *Desalination* 284 (2012) 253–260.
- [13] J.S. Yong, W.A. Phillip, M. Elimelech, Coupled reverse draw solute permeation and water flux in forward osmosis with neutral draw solutes, *J. Membr. Sci.* 392–393 (2012) 9–17.
- [14] G.T. Gray, J.R. McCutcheon, M. Elimelech, Internal concentration polarization in forward osmosis: Role of membrane orientation, *Desalination* 197(1–3) (2006) 1–8.
- [15] B. Mi, M. Elimelech, Chemical and physical aspects of organic fouling of forward osmosis membranes, *J. Membr. Sci.* 320(1–2) (2008) 292–302.
- [16] B. Mi, M. Elimelech, Organic fouling of forward osmosis membranes: Fouling reversibility and cleaning without chemical reagents, *J. Membr. Sci.* 348(1–2) (2010) 337–345.
- [17] E. Arkhangelsky, F. Wicaksana, S. Chou, A.A. Al-Rabiah, S.M. Al-Zahrani, R. Wang, Effects of scaling and cleaning on the performance of forward osmosis hollow fiber membranes, *J. Membr. Sci.* 415–416 (2012) 101–108.
- [18] V. Parida, H.Y. Ng, Forward osmosis organic fouling: Effects of organic loading, calcium and membrane orientation, *Desalination* 312 (2003) 88–98.
- [19] C. Boo, S. Lee, M. Elimelech, Z. Meng, S. Hong, Colloidal fouling in forward osmosis: Role of reverse salt diffusion, *J. Membr. Sci.* 390–391 (2012) 277–284.
- [20] Y. Liu, B. Mi, Combined fouling of forward osmosis membranes: Synergistic foulant interaction and direct observation of fouling layer formation, *J. Membr. Sci.* 407–408 (2012) 136–144.
- [21] J. Zhang, W.L.C. Loong, S. Chou, C. Tang, R. Wang, A.G. Fane, Membrane biofouling and scaling in forward osmosis membrane bioreactor, *J. Membr. Sci.* 403–404 (2012) 8–14.
- [22] S.-M. Park, J.-W. Koo, Y.-K. Choi, S. Lee, J. Sohn, T.-M. Hwang, Optimization of hybrid system consisting of forward osmosis and reverse osmosis: A Monte Carlo simulation approach, *Desalin. Water Treat.* 43(1–3) (2012) 274–280.
- [23] O.A. Bamaga, A. Yokochi, E.G. Beaudry, Application of forward osmosis in pretreatment of seawater for small reverse osmosis desalination units, *Desalin. Water Treat.* 5 (2009) 183–191.
- [24] J.-S. Choi, H. Kim, S. Lee, T.-M. Hwang, H. Oh, D.R. Yang, J. H. Kim, Theoretical investigation of hybrid desalination system combining reverse osmosis and forward osmosis, *Desalin. Water Treat.* 15 (2010) 114–120.
- [25] T.-S. Chung, S. Zhang, K.Y. Wang, J. Su, M.M. Ling, Forward osmosis processes: Yesterday, today and tomorrow, *Desalination* 287 (2012) 78–81.
- [26] S. Zhao, L. Zou, C.Y. Tang, D. Mulcahy, Recent developments in forward osmosis: Opportunities and challenges, *J. Membr. Sci.* 396 (2012) 1–21.
- [27] T.Y. Cath, A. Childress, M. Elimelech, Forward osmosis: Principles, applications, and recent developments, *J. Membr. Sci.* 281(1–2) (2006) 70–87.
- [28] L. Chekli, S. Phuntsho, H.K. Shon, S. Vigneswaran, J. Kandasamy, A. Chanan, A review of draw solutes in forward osmosis process and their use in modern applications, *Desalin. Water Treat.* 43(1–3) (2012) 167–184.
- [29] K. Lee, R. Baker, H. Lonsdale, Membranes for power generation by pressure-retarded osmosis, *J. Membr. Sci.* 8(2) (1981) 141–171.
- [30] S. Loeb, L. Titelman, E. Korngold, J. Freiman, Effect of porous support fabric on osmosis through a Loeb–Sourirajan type asymmetric membrane, *J. Membr. Sci.* 129(2) (1997) 243–249.
- [31] C.H. Tan, H.Y. Ng, Modified models to predict flux behavior in forward osmosis in consideration of external and internal concentration polarizations, *J. Membr. Sci.* 324(1–2) (2008) 209–219.
- [32] Jeffrey R. Mccutcheon, Menachem Elimelech, Modeling water flux in forward osmosis: Implications for improved membrane design, *AIChE J.* 53(7) (2007) 1736–1744.
- [33] A. Tiraferri, N.Y. Yip, W.A. Phillip, J.D. Schiffman, M. Elimelech, Relating performance of thin-film composite forward osmosis membranes to support layer formation and structure, *J. Membr. Sci.* 367(1–2) (2011) 340–352.
- [34] S. Zhao, L. Zou, Effects of working temperature on separation performance, membrane scaling and cleaning in forward osmosis desalination, *Desalination* 278(1–3) (2011) 157–164.
- [35] W.C.L. Lay, J. Zhang, C. Tang, R. Wang, Y. Liu, A.G. Fane, Factors affecting flux performance of forward osmosis systems, *J. Membr. Sci.* 394–395 (2012) 151–168.
- [36] D. Xiao, W. Li, S. Chou, R. Wang, C.Y. Tang, A modeling investigation on optimizing the design of forward osmosis hollow fiber modules, *J. Membr. Sci.* 392–393 (2012) 76–87.
- [37] D.H. Jung, J. Lee, D.Y. Kim, Y.G. Lee, M. Park, S. Lee, D.R. Yang, J.H. Kim, Simulation of forward osmosis membrane process: Effect of membrane orientation and flow direction of feed and draw solutions, *Desalination* 277(1–3) (2011) 83–91.
- [38] C. Zhao, J. Wang, Z. Luan, Preparation of high concentration polyaluminum chloride with high Al<sub>c</sub> content by membrane distillation, *Chinese J. Chem. Eng.* 19(1) (2011) 173–176.
- [39] W. Li, Y. Gao, C.Y. Tang, Network modeling for studying the effect of support structure on internal concentration polarization during forward osmosis: Model development and theoretical analysis with FEM, *J. Membr. Sci.* 379(1–2) (2011) 307–321.
- [40] M.F. Gruber, C.J. Johnson, C.Y. Tang, M.H. Jensen, L. Yde, C. Hélix-Nielsen, Computational fluid dynamics simulations of flow and concentration polarization in forward osmosis membrane systems, *J. Membr. Sci.* 379(1–2) (2011) 488–495.
- [41] A. Sagiv, R. Semiat, Finite element analysis of forward osmosis process using NaCl solutions, *J. Membr. Sci.* 379(1–2) (2011) 86–96.
- [42] J.S. Hansen, J.C. Dyre, Simplistic Coulomb forces in molecular dynamics: Comparing the Wolf and shifted-force approximations, *J. Phys. Chem. B* 116(19) (2012) 5738–5743.
- [43] S. Loeb, Production of energy from concentrated brines by pressure-retarded osmosis: I. Preliminary technical and economic correlations, *J. Membr. Sci.* 1 (1976) 49–63.
- [44] J.R. Mccutcheon, M. Elimelech, Influence of concentrative and dilutive internal concentration polarization on flux behavior in forward osmosis, *J. Membr. Sci.* 284 (2006) 237–247.
- [45] A.S. Kim, H. Chen, Diffusive tortuosity factor of solid and soft cake layers: A random walk simulation approach, *J. Membr. Sci.* 279(1–2) (2006) 129–139.
- [46] E. Lindahl, B. Hess, D.v.d. Spoel, GROMACS 3.0: A package for molecular simulation and trajectory analysis, *J. Mol. Model.* 7(8) (2001) 306–317.
- [47] N. Foloppe, A.D. MacKerell, Jr. All-atom empirical force field for nucleic acids: I. Parameter optimization based on small molecule and condensed phase macromolecular target data, *J. Comp. Chem.* 21(2) (2000) 86–104.
- [48] R.C. Rizzo, W.L. Jorgensen, OPLS all-atom model for amines: Resolution of the amine hydration problem, *J. Am. Chem. Soc.* 121(20) (1999) 4827–4836.
- [49] A.T. Brunger. X-PLOR Version 3.1 a System for X-ray Crystallography and NMR, Technical report, Yale University, New Haven, CT, 1993.
- [50] J. Wang, P. Cieplak, P.A. Kollman, How well does a restrained electrostatic potential (RESP) model perform in calculating conformational energies of organic and biological molecules, *J. Comp. Chem.* 21(12) (2000) 1049–1074.
- [51] D. Smith, L. Dang, Computer simulations of NaCl association in polarizable water, *J. Chem. Phys.* 100(5) (1994) 3757–3766.